Synthesis and singularity analysis of N-UU parallel wrists: A symmetric space approach

(Article begins on next page)

14 July 2024

Synthesis and Singularity Analysis of N-$\mathcal{UU}$ Parallel Wrists: a Symmetric Space Approach*

Yuanqing Wu[†]
Department of Industrial Engineering
University of Bologna
Via Risorgimento 2, Bologna 40136
Email: yuanqing.wu@unibo.it

Marco Carricato
Department of Industrial Engineering
University of Bologna
Via Risorgimento 2, Bologna 40136
Email: marco.carricato@unibo.it

We report some recent advances in kinematics and singularity analysis of the mirror-symmetric N-$\mathcal{UU}$ parallel wrists using symmetric space theory. We show that both the finite displacement and infinitesimal singularity kinematics of a N-$\mathcal{UU}$ wrist are governed by the mirror-symmetry property and half-angle property of the underlying motion manifold, which is a symmetric submanifold of the special Euclidean group SE(3). Our result is stronger than and may be considered a closure of Hunt's argument for instantaneous mirror-symmetry in his pioneering exposition of constant velocity shaft couplings. Moreover, we show that the wrist can to some extent be treated as a spherical mechanism, even though dependent translation exists, and the singularity-free workspace of a N-$\mathcal{UU}$ wrist may be analytically derived. This leads to a straightforward optimal design for maximal singularity-free workspace.

Nomenclature

$\mathcal{R}$ revolute joint
$\mathcal{U}$ universal joint formed by two concurrent $\mathcal{R}$ joints
o-xyz   reference coordinate frame
$\mathbf{x}, \mathbf{y}, \mathbf{z}$ $(1,0,0)^T, (0,1,0)^T, (0,0,1)^T$
$\mathbf{u}, \mathbf{v}, \mathbf{w}, \mathbf{s}, \mathbf{t}, \mathbf{0}, \dots$ 3-d vectors / points
$\mathbf{s}^+$ proximal center in the base
$\mathbf{s}^-$ distal center in the end-effector
$\xi, \zeta, \eta, \dots$ unit screws
$\widehat{\mathbf{w}}$ 3×3 skew symmetric matrix s.t. $\widehat{\mathbf{w}}\mathbf{v} = \mathbf{w} \times \mathbf{v}, \forall \mathbf{v} \in \mathbb{R}^3$
$\widehat{\xi}$ 4×4 homogeneous matrix form of a screw ξ [1]
$c_{(\cdot)}, s_{(\cdot)}$ $\cos(\cdot), \sin(\cdot)$

SO(3)   spatial rotation group
$$SO(3) := \left\{ \mathbf{R} \in \mathbb{R}^{3 \times 3} \mid \mathbf{R}\mathbf{R}^T = \mathbf{1}_{3 \times 3}, \det \mathbf{R} = 1 \right\}$$
SE(3)   special Euclidean group (homogeneous rep.)
$$SE(3) := \left\{ \begin{pmatrix} \mathbf{R} & \mathbf{t} \\ \mathbf{0}^T & 1 \end{pmatrix} \in \mathbb{R}^{4 \times 4} \mid \mathbf{R} \in SO(3), \mathbf{t} \in \mathbb{R}^3 \right\}$$
$(\mathbf{R})_H$ homogeneous embedding of $\mathbf{R} \in SO(3)$
$$(\mathbf{R})_H := \begin{pmatrix} \mathbf{R} & \mathbf{0} \\ \mathbf{0}^T & 1 \end{pmatrix}$$
$(\mathbf{t})_H$ homogeneous embedding of $\mathbf{t} \in \mathbb{R}^3$
$$(\mathbf{t})_H := \begin{pmatrix} \mathbf{1}_{3 \times 3} & \mathbf{t} \\ \mathbf{0}^T & 1 \end{pmatrix}$$
$e^{\theta \widehat{\mathbf{w}}} \in SO(3)$ rotation matrix with unit axis $\mathbf{w}$ and magnitude θ
$e^{\theta \widehat{\xi}} \in SE(3)$ rigid transformation matrix with unit screw axis ξ and magnitude θ
(ϕ, ψ, σ) tilt-torsion angle parameters for rotation matrix $\mathbf{R}$
$\quad \mathbf{R} = e^{\psi(c_\phi \widehat{\mathbf{x}} + s_\phi \widehat{\mathbf{y}})} e^{\sigma \widehat{\mathbf{z}}}$
ξ_{ij}^+ $(i = 1, \dots, N, \ j = 1, 2)$ revolute axes (unit screws) of the proximal $\mathcal{U}$ joint in leg i
ξ_{ij}^- $(i = 1, \dots, N, \ j = 1, 2)$ revolute axes of the distal $\mathcal{U}$ joint in leg i (ξ_{ij}^+ and ξ_{ij}^-, $j = 1, 2$ are mirror-symmetric about a common plane)
$\mathbf{w}_{ij}^{\pm}$ $(i = 1, \dots, N, \ j = 1, 2)$ unit direction vector of $\xi_{ij}^{\pm}$
$\mathbf{s}_{ij}$ $(i = 1, \dots, N, \ j = 1, 2)$ intersection point of ξ_{ij}^+ and ξ_{ij}^- (may be located at infinity)
$\theta_{ij}^{\pm}$ $(i = 1, \dots, N, \ j = 1, 2)$ joint variable of $\xi_{ij}^{\pm}$
$\mathbf{w}_{EE}$ angular velocity vector of the end-effector
d distance between $\mathbf{o}$ and $\mathbf{s}^+$ (or $\mathbf{s}^-$)
α angle formed by the two planes containing $\xi_{i1}^{\pm}$ and $\xi_{i2}^{\pm}$, respectively (at the initial configuration)
β angle formed by ξ_{i1}^+ (or ξ_{i1}^-) and the **xy**-plane (at the initial configuration)
γ half the angle formed by ξ_{i2}^+ and ξ_{i2}^-
μ angle formed by ξ_{i1}^+ and ξ_{i2}^+ (or ξ_{i1}^- and ξ_{i2}^-)

[†]Address all correspondence to this author.

$\mathbf{s}_1\mathbf{s}_2$, $\mathbf{s}_1\mathbf{s}_2\mathbf{s}_3$ ($\mathbf{s}_i$, $i = 1, 2, 3$ being 3-d points) extensor of step 2 and 3 (Grassmann-Cayley algebra), i.e. a line through $\mathbf{s}_1, \mathbf{s}_2$ and a plane through $\mathbf{s}_1, \mathbf{s}_2, \mathbf{s}_3$ respectively

$\wedge$ meet operator (Grassmann-Cayley algebra), i.e. intersection of two operands

$\psi_L/\psi_A/\psi_P$ maximal half-tilt angle free of leg/ active/ passive singularities

1 INTRODUCTION

We report in this paper some recent advances in synthesis and analysis of parallel mechanisms (PMs) comprising N (N $\geq$ 3) $\mathcal{UU}$ legs using tools from symmetric space theory [2]. It is well known from theory of homokinetic couplings [3, 4] that the N-$\mathcal{UU}$ PM has two rotational degrees-of-freedom (DoF) and is overconstrained (by a degree of $(2N - 4)$). The *synthesis condition* of N-$\mathcal{UU}$ PM is studied in [3, 4] and may be summarized as follows: *(i) the two $\mathcal{U}$ joints in each $\mathcal{UU}$ leg must be identical and remain in a mirror-symmetric configuration during full-cycle motion; (ii) all $\mathcal{UU}$ legs share the same plane of symmetry and the revolute axes of the proximal (or distal) $\mathcal{U}$ joints of all legs intersect at one point* (see Fig. 1 for the schematic of a 3-$\mathcal{UU}$ PM). However, the deduction of such conditions in [3] or [4] relies on instantaneous screw theory, which must be accompanied with full-cycle (finite instead of instantaneous) motion validation in the case of structural design. Wu *et al.* [5] gave an explicit expression for the (finite full-cycle) motion manifold of N-$\mathcal{UU}$ PMs using tilt-torsion angle parameters [6]. Indeed, the N-$\mathcal{UU}$ PM is shown to be a zero-torsion PM, a concept often associated with 2- or 3-DoF homokinetic-coupling-equivalent PMs [7]. N-$\mathcal{UU}$ PMs have been discovered [8] and and rediscovered [9–11] as homokinetic couplings or robotic wrists in several occasions.

Recently, we sharpened our previous results [4,5] to provide a deeper understanding of the synthesis and analysis of homokinetic couplings [2, 12, 13]. This recent advance involves recognizing the motion manifolds of the homokinetic couplings, including the N-$\mathcal{UU}$ PMs, as members of a special class of submanifolds of the special Euclidean group SE(3), called *symmetric submanifolds*. For example, the collection of all zero-torsion rotation matrices [6, 7]

$$\mathrm{M} := \left\{ e^{\psi\widehat{\mathbf{w}}} \ \Big| \ \mathbf{w} = \mathbf{x}c_\phi + \mathbf{y}s_\phi, \ \phi \in [0, 2\pi), \ \psi \in [0, \pi] \right\} \quad (1)$$

is in fact one of the seven symmetric submanifolds of SE(3) [2]. The general theory is rather sophisticated, and shall not be re-introduced here. A more accessible treatment of the 2-d symmetric submanifold M may be found in [14]. Instead, we show in this paper that two important consequences of the symmetric space theory, namely a *full-cycle* version of the *mirror-symmetry property* [3] and the *half-angle property* (see Sec. 2), lead to a rigorous treatment of the synthesis and analysis of N-$\mathcal{UU}$ PMs. Moreover, we show that a N-$\mathcal{UU}$ PM, although not a purely spherical mechanism (in the sense that its motion manifold is not exactly M as defined in Eqn. (1)), may in fact be synthesized and analyzed as one.

A particular example of the latter can be found in our earlier presentation [15].

The following references are also relevant to our work. Sofka *et al.* [16] are probably the first to study the displacement kinematics of a 4-$\mathcal{UU}$ parallel wrist. Since mirror symmetry is not utilized, a genetic algorithm has to be implemented to solve the problem. Yu *et al.* [17, 18] studied the mobility, singularity and synthesis of N-$\mathcal{UU}$ parallel wrists using reciprocal screw theory and structural symmetry. Their work is essentially an extension to Hunt's instantaneous approach [3], where the underlying full-cycle motion manifold is not revealed; nor did they address the singularity-free workspace characterization and optimization problem. Kong *et al.* [11, 19] studied the synthesis and reconfiguration of multi-mode N-$\mathcal{UU}$ PMs resulting from imposing plane symmetric conditions on a 2-DoF 3-$\mathcal{UU}$ PM obtained by locking three joints of a 5-DoF parallel mechanism. A mode change occurs when mirror-symmetry is broken. Bonev *et al.* [20, 21] used tilt-torsion angle parameters to characterize the singularity loci of 2- to 3-DoF spherical manipulators.

This paper is organized as follows. In Sec. 2, we revisit the synthesis condition of N-$\mathcal{UU}$ PMs by using symmetric space theory. We show that many subtle conclusions may be immediately drawn without pounding on the particular geometry of the N-$\mathcal{UU}$ PM. In Sec. 3, we perform a full singularity analysis of the N-$\mathcal{UU}$ PM treated as a spatial mechanism, using Grassmann-Cayley algebra (GCA) [22, 23]. The results are then compared with those concerning its pure rotational counterpart [15] to illustrate our claim that the N-$\mathcal{UU}$ PM can be essentially treated as a purely rotational mechanism. In Sec. 4, we derive the singularity loci of N-$\mathcal{UU}$ PMs and identify maximal singularity-free tilt angle for a particular choice of design constants. Finally, in Sec. 5 we conduct optimal design of N-$\mathcal{UU}$ PMs for maximal singularity-free workspace.

2 Geometry and Synthesis Condition of N-$\mathcal{UU}$ PM
2.1 Geometry of $\mathcal{UU}$ Leg

In its most general form (Fig. 1(c)), the i-th $\mathcal{UU}$ leg of a N-$\mathcal{UU}$ PM comprises two pairs of $\mathcal{R}$ joints, $(\boldsymbol{\xi}_{i1}^+, \boldsymbol{\xi}_{i1}^-)$ and $(\boldsymbol{\xi}_{i2}^+, \boldsymbol{\xi}_{i2}^-)$, which are both mirror-symmetric about the **xy**-plane. We denote their intersection with the **xy**-plane by $\mathbf{s}_{i1}$ and $\mathbf{s}_{i2}$ respectively. We denote the centers of the proximal and distal $\mathcal{U}$ joints, respectively, by $\mathbf{s}^+$ and $\mathbf{s}^-$, which are also mirror-symmetric about the **xy**-plane. Assume, without loss of generality, that the N-$\mathcal{UU}$ PM has N identical $\mathcal{UU}$ legs forming an N-fold axial symmetry about the **z** axis. It is not difficult to see that the length parameter d (measuring the distance between **o** and $\mathbf{s}^+$ or $\mathbf{s}^-$) and three angular constants (α, β, γ) completely determine the kinematic geometry of the $\mathcal{UU}$ leg:

$$\begin{aligned}
\boldsymbol{\xi}_{i1}^+ &= ((\mathbf{w}_{i1}^+)^T, (\mathbf{s}^+ \times \mathbf{w}_{i1}^+)^T)^T \\
\boldsymbol{\xi}_{i1}^- &= ((\mathbf{w}_{i1}^-)^T, (\mathbf{s}^- \times \mathbf{w}_{i1}^-)^T)^T \\
\boldsymbol{\xi}_{i2}^+ &= ((\mathbf{w}_{i2}^+)^T, (\mathbf{s}^+ \times \mathbf{w}_{i2}^+)^T)^T \\
\boldsymbol{\xi}_{i2}^- &= ((\mathbf{w}_{i2}^-)^T, (\mathbf{s}^- \times \mathbf{w}_{i2}^-)^T)^T
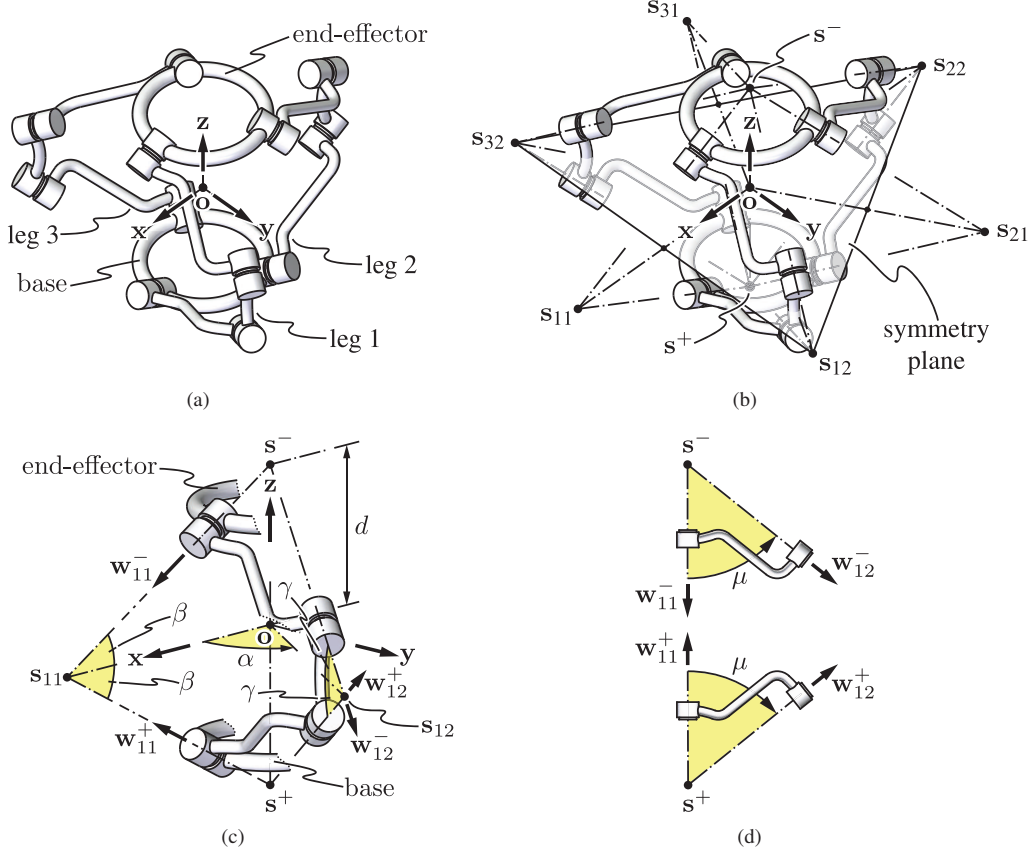\end{aligned} \quad (2)$$

Fig. 1. Schematic of a general 3-$\mathcal{UU}$ PM: (a) components of the PM; (b) synthesis condition of the PM: the two $\mathcal{U}$ joints in each leg are mirror-symmetric about the **xy**-plane, and the revolute axes of all proximal (or distal) $\mathcal{U}$ joints in all legs intersect at a point $\mathbf{s}^+$ (or $\mathbf{s}^-$); (c) geometry of the first leg; (d) geometry of the $\mathcal{U}$ joints in the first leg.

with

$$\mathbf{w}_{i1}^+ = e^{(2\pi(i-1)/N)\widehat{\mathbf{z}}} e^{-\beta\widehat{\mathbf{y}}} \cdot \mathbf{x}$$

$$\mathbf{w}_{i1}^- = e^{(2\pi(i-1)/N)\widehat{\mathbf{z}}} e^{\beta\widehat{\mathbf{y}}} \cdot \mathbf{x} \qquad \mathbf{s}^+ = -d\mathbf{z}$$

$$\mathbf{w}_{i2}^+ = e^{(\alpha+2\pi(i-1)/N)\widehat{\mathbf{z}}} e^{-\gamma\widehat{\mathbf{y}}} \cdot \mathbf{x} \qquad \mathbf{s}^- = d\mathbf{z} \qquad (3)$$

$$\mathbf{w}_{i2}^- = e^{(\alpha+2\pi(i-1)/N)\widehat{\mathbf{z}}} e^{\gamma\widehat{\mathbf{y}}} \cdot \mathbf{x}$$

The explanation for these constants can be found in the Nomenclature and Fig. 1(c). The two $\mathcal{R}$ joints in each $\mathcal{U}$ joint form the angle μ (Fig. 1(d)), which can be easily computed as

$$c_\mu = c_\alpha c_\beta c_\gamma + s_\beta s_\gamma \qquad (4)$$

For the study of the orientation workspace, the length parameter d is not essential and can be simply set to 1.

2.2 Symmetric Submanifold Properties of a Collapsed $\mathcal{UU}$ Leg

Consider the spherical chain resulting from collapsing $\mathbf{s}^\pm$ to **o** (or by letting $d = 0$), as shown in Fig. 2(a). If symmetric motion is enforced within the $\mathcal{R}$ joints of symmetric

pairs, the collapsed chain is known as a *symmetric chain* of the 2-d screw system $\mathfrak{m} := \text{span}(\widehat{\mathbf{x}}, \widehat{\mathbf{y}})$ (named $\mathfrak{m}_{2B}$ in [2]), characterized by a pencil of lines passing through **o** and lying in the **xy**-plane (Hunt's first special two-system with zero principal pitches [24]; see Fig. 2(c)). We summarize from [2] the following results for $\mathfrak{m}$ and M given in Eqn. (1) without a complete proof:

P1. The submanifold M in Eqn. (1) is the exponential image of the two-system $\mathfrak{m}$, $M = \exp\mathfrak{m}$. M remains invariant under rotation about the **z**-axis, i.e. $\forall\phi_0 \in [0, 2\pi)$:

$$e^{\phi_0\widehat{\mathbf{z}}} M e^{-\phi_0\widehat{\mathbf{z}}} = e^{\phi_0\widehat{\mathbf{z}}} (\exp\mathfrak{m}) e^{-\phi_0\widehat{\mathbf{z}}} = \exp(e^{\phi_0\widehat{\mathbf{z}}}\mathfrak{m}e^{-\phi_0\widehat{\mathbf{z}}})$$
$$= \exp(\text{span}(e^{\phi_0\widehat{\mathbf{z}}}\widehat{\mathbf{x}}e^{-\phi_0\widehat{\mathbf{z}}}, e^{\phi_0\widehat{\mathbf{z}}}\widehat{\mathbf{y}}e^{-\phi_0\widehat{\mathbf{z}}}))$$
$$= \exp(\text{span}(\widehat{e^{\phi_0\widehat{\mathbf{z}}}\mathbf{x}}, \widehat{e^{\phi_0\widehat{\mathbf{z}}}\mathbf{y}}))$$
$$= \exp(\text{span}(\widehat{\mathbf{x}}c_{\phi_0} + \widehat{\mathbf{y}}s_{\phi_0}, \widehat{\mathbf{y}}c_{\phi_0} - \widehat{\mathbf{x}}s_{\phi_0}))$$
$$= \exp(\text{span}(\widehat{\mathbf{x}}, \widehat{\mathbf{y}})) = M \qquad (5)$$

We say that M has an axial symmetry.

P2. For any leg i, so long as the projection of $\mathbf{w}_{i1}^\pm$ and $\mathbf{w}_{i2}^\pm$ onto the **xy**-plane are linearly independent (for example, in the configuration shown in Fig. 2(b)), the symmetric chain $(\mathbf{w}_{i1}^+, \mathbf{w}_{i2}^+, \mathbf{w}_{i2}^-, \mathbf{w}_{i1}^-)$ generates M under the symmetric movement condition $\theta_{ij}^+ = \theta_{ij}^- = \theta_{ij}$, $j = 1, 2$, i.e., for
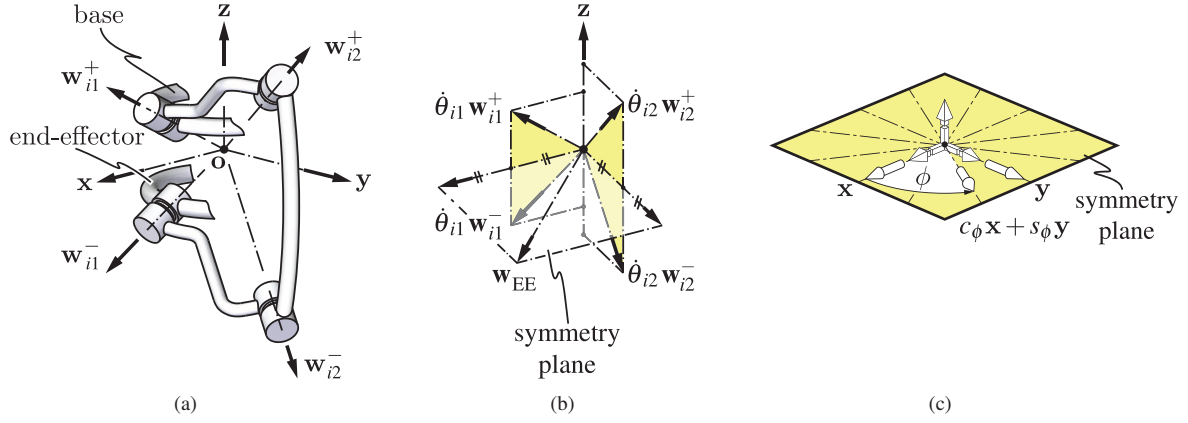
Fig. 2. Collapsing of a $\mathcal{UU}$ leg to a symmetric spherical chain: (a) schematic; (b) instantaneous symmetric movement ($\dot{\theta}_{1j}^+ = \dot{\theta}_{1j}^- = \dot{\theta}_{1j}$, $j = 1,2$); (c) screw system of the corresponding LTS $\mathfrak{m}$: a planar pencil of zero-pitch screws.

any tilt axis $\mathbf{w} = \mathbf{x}c_\phi + \mathbf{y}s_\phi$, $\phi \in [0, 2\pi)$, and *half-tilt angle* ψ (within a singularity-free workspace; see Sec. 3), we may find a unique pair $(\theta_{i1}, \theta_{i2}) \in [0, 2\pi)^2$, such that

$$e^{\theta_{i1}\widehat{\mathbf{w}}_{i1}^+}e^{\theta_{i2}\widehat{\mathbf{w}}_{i2}^+}e^{\theta_{i2}\widehat{\mathbf{w}}_{i2}^-}e^{\theta_{i1}\widehat{\mathbf{w}}_{i1}^-} = e^{2\psi\widehat{\mathbf{w}}} \in \mathrm{M} \quad (6)$$

P1 and P2 imply that arbitrarily displacing the symmetric chain (under symmetric movement condition) by a rotation about the $\mathbf{z}$-axis does not alter its motion manifold M.

P3. Under the aforementioned symmetric movement condition, at a generic configuration $e^{2\psi\widehat{\mathbf{w}}}$, the symmetric chain will be always mirror-symmetric about its instantaneous velocity plane, which passes through $\mathbf{o}$ and is perpendicular to $e^{\psi\widehat{\mathbf{w}}}\mathbf{z}$. Moreover, there exists some $\sigma_i \in \mathbb{R}$ such that [15]:

$$\begin{aligned} e^{\theta_{i1}\widehat{\mathbf{w}}_{i1}^+}e^{\theta_{i2}\widehat{\mathbf{w}}_{i2}^+} &= e^{\psi\widehat{\mathbf{w}}}e^{\sigma_i\widehat{\mathbf{z}}} \\ e^{-\theta_{i1}\widehat{\mathbf{w}}_{i1}^-}e^{-\theta_{i2}\widehat{\mathbf{w}}_{i2}^-} &= e^{-\psi\widehat{\mathbf{w}}}e^{\sigma_i\widehat{\mathbf{z}}} \end{aligned} \quad (7)$$

so that

$$e^{\theta_{i1}\widehat{\mathbf{w}}_{i1}^+}e^{\theta_{i2}\widehat{\mathbf{w}}_{i2}^+} \cdot \mathbf{z} = e^{\psi\widehat{\mathbf{w}}} \cdot \mathbf{z} \quad (8)$$

In other words, the symmetry plane may be thought of as being rigidly attached to the central link of the collapsed $\mathcal{UU}$ leg. This information will be very useful for singularity analysis.

The aforementioned properties of M are a direct consequence of M being a *symmetric submanifold* of SE(3) and $\mathfrak{m}$ being its associated *Lie triple subsystem* (LTS) [2, 13]. More specifically, the correspondence between $\mathfrak{m}$ and M in P1 is a generalization of the Lie correspondence between a Lie algebra and its corresponding Lie group [2]. The second claim in P1 is due to the fact that $\mathfrak{m}$ is invariant under the adjoint action of its corresponding commutator algebra [2].

A systematic treatment of symmetric chains for all symmetric submanifolds of SE(3) as in P2 is given in [2]. P3 is also generalizable to general symmetric submanifolds with $\psi\widehat{\mathbf{w}}$ replaced by a vector in a general LTS $\mathfrak{m}$ and $\sigma\widehat{\mathbf{z}}$ by a vector in its corresponding commutator algebra [2]. We also remark that, Hunt's screw argument [3] may be summarized as (see Fig. 2(b))

$$\dot{\theta}_{i1}\mathbf{w}_{i1}^+ + \dot{\theta}_{i1}\mathbf{w}_{i1}^- + \dot{\theta}_{i2}\mathbf{w}_{i2}^+ + \dot{\theta}_{i2}\mathbf{w}_{i2}^- = \mathbf{w}_{\mathrm{EE}} \in \mathfrak{m} \quad (9)$$

which is an instantaneous and therefore weaker version of Eqn. (6). In reference to P1 and P2, one may simply construct a "collapsed" N-$\mathcal{UU}$ PM by arranging several copies of the symmetric chain $(\mathbf{w}_{11}^+, \mathbf{w}_{12}^+, \mathbf{w}_{12}^-, \mathbf{w}_{11}^-)$ in parallel, with each copy being obtained by a rotation about the $\mathbf{z}$-axis by some angle ϕ_0.

2.3 Synthesis Condition of N-$\mathcal{UU}$ PM

Now we prove the synthesis condition for N-$\mathcal{UU}$ PMs, using a generalized version of P1 for M. We notice that for any $i \in \{1, 2, \ldots, N\}$ and $j = 1, 2$:

$$e^{\theta_{ij}\widehat{\xi}_{ij}^\pm} = (\mp d\mathbf{z})_{\mathrm{H}} \cdot (e^{\theta_{1j}\widehat{\mathbf{w}}_{ij}^\pm})_{\mathrm{H}} \cdot (\pm d\mathbf{z})_{\mathrm{H}} \quad (10)$$

The non-collapsing $\mathcal{UU}$ leg generates, under symmetric movement condition,

$$\begin{aligned} & e^{\theta_{i1}\widehat{\xi}_{i1}^+}e^{\theta_{i2}\widehat{\xi}_{i2}^+}e^{\theta_{i2}\widehat{\xi}_{i2}^-}e^{\theta_{i1}\widehat{\xi}_{i1}^-} \\ =& (-d\mathbf{z})_{\mathrm{H}} \cdot (e^{\theta_{i1}\widehat{\mathbf{w}}_{i1}^+})_{\mathrm{H}} \cdot (e^{\theta_{i2}\widehat{\mathbf{w}}_{i2}^+})_{\mathrm{H}} \cdot (d\mathbf{z})_{\mathrm{H}} \cdots \\ & (d\mathbf{z})_{\mathrm{H}} \cdot (e^{\theta_{i2}\widehat{\mathbf{w}}_{i2}^-})_{\mathrm{H}} (e^{\theta_{i1}\widehat{\mathbf{w}}_{i1}^-})_{\mathrm{H}} \cdot (-d\mathbf{z})_{\mathrm{H}} \\ =& (-d\mathbf{z})_{\mathrm{H}} \cdot (e^{\psi\widehat{\mathbf{w}}})_{\mathrm{H}} \cdot (e^{\sigma\widehat{\mathbf{z}}})_{\mathrm{H}} \cdot (2d\mathbf{z})_{\mathrm{H}} \cdots \\ & (e^{-\sigma\widehat{\mathbf{z}}})_{\mathrm{H}} \cdot (e^{\psi\widehat{\mathbf{w}}})_{\mathrm{H}} \cdot (-d\mathbf{z})_{\mathrm{H}} \\ =& (-d\mathbf{z})_{\mathrm{H}} \cdot (e^{\psi\widehat{\mathbf{w}}})_{\mathrm{H}} \cdot (2d\mathbf{z})_{\mathrm{H}} \cdot (e^{\psi\widehat{\mathbf{w}}})_{\mathrm{H}} \cdot (-d\mathbf{z})_{\mathrm{H}} \end{aligned} \quad (11)$$

The last equality is due to $(a\mathbf{z})_H$ commuting with $(e^{b\hat{\mathbf{z}}})_H$ for any $a \in \mathbb{R}$ and $b \in [0, 2\pi]$. Equation (11) directly leads to the explicit expression for the motion manifold M_d of the non-collapsing $\mathcal{UU}$ leg (under symmetric movement condition)

$$M_d := \left\{ (-d\mathbf{z})_H \cdot (e^{\psi\hat{\mathbf{w}}})_H \cdot (2d\mathbf{z})_H \cdot (e^{\psi\hat{\mathbf{w}}})_H \cdot (-d\mathbf{z})_H \mid \ldots \right.$$
$$\left. \mathbf{w} = \mathbf{x}c_\phi + \mathbf{y}s_\phi, \phi \in [0, 2\pi), \psi \in [0, \pi] \right\} \tag{12}$$

Again by commutativity of $(a\mathbf{z})_H$ and $(e^{b\hat{\mathbf{z}}})_H$, $\forall a \in \mathbb{R}, b \in [0, 2\pi)$, M_d also admits an axial symmetry, which follows from that of M. We may therefore construct an N-$\mathcal{UU}$ PM with legs being copies of a $\mathcal{UU}$ leg rotated about the $\mathbf{z}$-axis by different angles ϕ_0, so long as the *force matching condition* [25, Prop. 6] is satisfied, i.e., the PM is away from passive constraint singularities (see Sec. 3.3). We emphasize that the force matching condition is essential to our claim: each $\mathcal{UU}$ leg before assembly is not guaranteed to move under the symmetric movement condition, and in general it generates a 4-d submanifold of SE(3) that contains the desired 2-d motion manifold M_d. Consequently, the motion manifold of the N-$\mathcal{UU}$ PM may also be bigger than M_d. This is impossible if the force matching condition holds. Therefore, without loss of generality, we may synthesize a N-$\mathcal{UU}$ PM with identical and evenly distributed $\mathcal{UU}$ legs. Figure 1 shows one such PM with N = 3.

Note that the same conclusion is reached in [5] using brute force computation. Here, we reveal the axial symmetry more elegantly using commutativity of coaxial translation and rotation. We would like to draw a connection between this new approach and some recent work of Selig [26], where the role of commutativity in synthesis of several novel mechanisms is emphasized.

3 Kinematics and Singularity Analysis of N-$\mathcal{UU}$ PM

In this section, we generalize P2 and P3 for M to M_d, for the purpose of kinematics and singularity analysis of N-$\mathcal{UU}$ PMs.

P2′ The symmetric chain $(\xi_{i1}^+, \xi_{i2}^+, \xi_{i2}^-, \xi_{i1}^-)$ generates M_d under symmetric movement condition $\theta_{ij}^+ = \theta_{ij}^- = \theta_{ij}$, $j = 1, 2$, i.e., for any tilt axis $\mathbf{w} = \mathbf{x}c_\phi + \mathbf{y}s_\phi$, $\phi \in [0, 2\pi)$ and half-tilt angle ψ (within a singularity-free workspace; see Sec. 3), we may find a unique pair $(\theta_{i1}, \theta_{i2}) \in [0, 2\pi)^2$, such that

$$e^{\theta_{i1}\hat{\xi}_{i1}^+} e^{\theta_{i2}\hat{\xi}_{i2}^+} e^{\theta_{i2}\hat{\xi}_{i2}^-} e^{\theta_{i1}\hat{\xi}_{i1}^-} =$$
$$(-d\mathbf{z})_H \cdot (e^{\psi\hat{\mathbf{w}}})_H \cdot (2d\mathbf{z})_H \cdot (e^{\psi\hat{\mathbf{w}}})_H \cdot (-d\mathbf{z})_H \tag{13}$$

P3′ Under the aforementioned symmetric movement condition, at a generic configuration $(-d\mathbf{z})_H \cdot (e^{\psi\hat{\mathbf{w}}})_H \cdot (2d\mathbf{z})_H \cdot (e^{\psi\hat{\mathbf{w}}})_H \cdot (-d\mathbf{z})_H$, the symmetric chain will always be mirror-symmetric about its instantaneous ve-

locity plane, which passes through a point $\underline{\mathbf{o}}$ given by

$$\underline{\mathbf{o}} := e^{\theta_{i1}\hat{\xi}_{i1}^+} e^{\theta_{i2}\hat{\xi}_{i2}^+} \cdot \mathbf{o} = (-d\mathbf{z})_H \cdot (e^{\psi\hat{\mathbf{w}}})_H \cdot (d\mathbf{z})_H \cdot \mathbf{o}$$
$$= (e^{\psi\hat{\mathbf{w}}} - \mathbf{1}_{3\times3}) \cdot d\mathbf{z} \tag{14}$$

and is perpendicular to $e^{\psi\hat{\mathbf{w}}}\mathbf{z}$. In other words, the symmetry plane may be thought of as being rigidly attached to the central link of the $\mathcal{UU}$ leg. Moreover, we have

$$\underline{\mathbf{o}} - \mathbf{s}^+ = (e^{\psi\hat{\mathbf{w}}} - \mathbf{1}_{3\times3}) \cdot d\mathbf{z} - (-d\mathbf{z}) = e^{\psi\hat{\mathbf{w}}} \cdot d\mathbf{z} \tag{15}$$

By mirror-symmetry, $\mathbf{s}^- - \mathbf{s}^+ = e^{\psi\hat{\mathbf{w}}} \cdot 2d\mathbf{z}$. In other words, the distal center $\mathbf{s}^-$ rotates about the fixed proximal center $\mathbf{s}^+$, with unit direction vector $\mathbf{w}$ (same as that of the end-effector) and magnitude ψ (half that of the end-effector); $\underline{\mathbf{o}}$ remains the center of the line segment $\mathbf{s}^- - \mathbf{s}^+$ (with a fixed length of $2d$) under full-cycle motion (see Fig. 3(a)).

We remark that P2′ is a direct consequence of Eqn. (11); P3′ may be verified by straightforward computation, or alternatively by treating the $\mathcal{UU}$ leg as an incomplete symmetric chain of certain 3-DoF LTS [2, Ex.3].

3.1 Displacement Kinematics

It is clear from Eqn. (13) that the end-effector motion of a N-$\mathcal{UU}$ PM is uniquely determined by its rotation matrix $e^{2\psi\hat{\mathbf{w}}}$, which in turn is determined by the inclination of $\mathbf{s}^- - \mathbf{s}^+$ away from the $\mathbf{z}$-axis (see Fig. 3(a)). This immediately leads to simple analytic derivation of both direct and inverse displacement kinematics, and the details are given in Appendix A.

3.2 Twist and Wrench Systems of N-$\mathcal{UU}$ PM

In reference to the mirror-symmetry property under symmetric movement condition, the instantaneous twist space will always be a zero-pitch twist (i.e., a pure rotation) from the line pencil located at $\underline{\mathbf{o}}$ in the symmetry plane, as shown by green arrows in Fig. 3(c). To maintain this instantaneous zero-torsion motion, we need a reciprocal wrench system of dimension 4, spanned by a 3-d wrench field (comprising zero-pitch wrenches lying in the symmetry plane and an infinite-pitch wrench perpendicular to the symmetry plane) and a zero-pitch wrench on $\mathbf{s}^+\mathbf{s}^-$.

Since the symmetric pairs (ξ_{i1}^+, ξ_{i1}^-) and (ξ_{i2}^+, ξ_{i2}^-) always intersect at two points, $\mathbf{s}_{i1}$ and $\mathbf{s}_{i2}$ respectively on the symmetry plane, it is straightforward to see that each $\mathcal{UU}$ leg contributes to a 2-d constraint wrench system spanned by two zero-pitch wrenches, with one passing through $\mathbf{s}_{i1}$ and $\mathbf{s}_{i2}$ (denoted ζ_{i1}) and the other passing through $\mathbf{s}^+$ and $\mathbf{s}^-$ (denoted ζ_2) (see Fig. 3(a), where the constraint wrenches are denoted by blue arrows). ζ_2 is identical for all legs [4]. This shows that at least three $\mathcal{UU}$ legs are needed to provide the required constraint wrench system: as shown in Fig. 3(b), ζ_{11}, ζ_{21} and ζ_{31} necessarily span the wrench field lying on
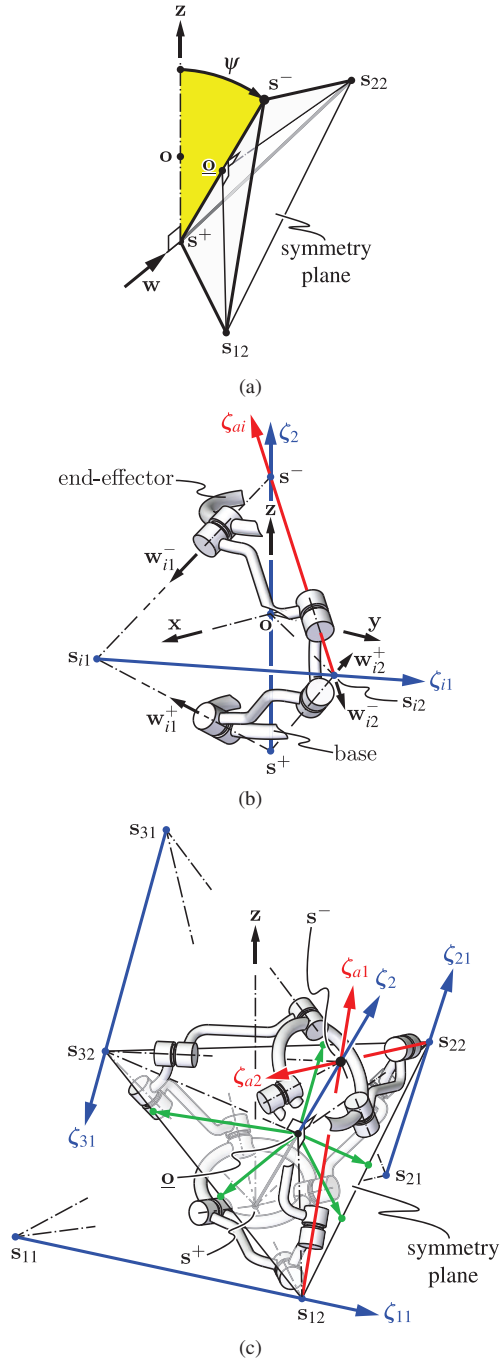
(a)

(b)

(c)

Fig. 3. (a) displacement kinematics of the 3-$\mathcal{UU}$ PM (leg 1 is hidden for clarity); (b) constraint wrenches (blue) and actuation wrenches (red) of leg i at initial configuration; (c) twists (green), constraint wrenches and actuation wrenches of the 3-$\mathcal{UU}$ PM.

the symmetry plane so long as they do not intersect at one point. The other basis wrench is fulfilled by ζ_2 of any $\mathcal{UU}$ leg.

Next, without loss of generality, consider the imposition of actuation wrenches ζ_{a1} and ζ_{a2} when choosing ξ_{11}^+ and ξ_{21}^+ as the two actuation joints. It is straightforward to verify that ζ_{a1} and ζ_{a2} may be chosen as the zero-pitch wrenches lying on $\mathbf{s}_{12}\mathbf{s}^-$ and $\mathbf{s}_{22}\mathbf{s}^-$ respectively, as illustrated by the red
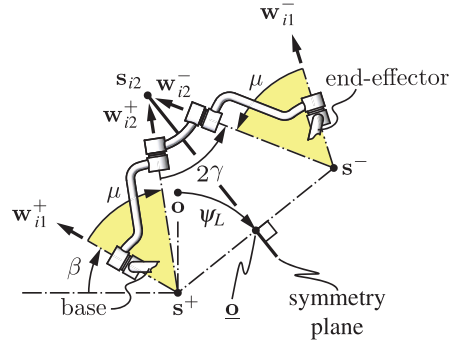

Fig. 4. A configuration of leg singularity of a $\mathcal{UU}$ leg.

arrows in Fig. 3(b) and (c).

3.3 Singularity analysis of N-$\mathcal{UU}$ PMs
Leg Singularity

A configuration of *leg singularity* corresponds to the linear dependency of all joint screws in a leg [27]. Since the N-$\mathcal{UU}$ PM operates and therefore approaches singularity with mirror-symmetry, it is not difficult to see that leg singularity occurs exactly when all four joint screws in a $\mathcal{UU}$ leg become coplanar, one particular configuration of which is shown in Fig. 4. This is necessarily a *stationary configuration* [24, 27] of the N-$\mathcal{UU}$ PM. Note that a leg singularity such as shown in Fig. 4 is achieved with a particular value of θ_{i2} but an arbitrary value of θ_{i1}. This implies that the $\mathcal{UU}$ leg may experience a continuous leg singularity by fixing θ_{i2} and continuously changing θ_{i1}.

Since we are interested in identifying the maximal singularity-free workspace, we identify the leg singularity that achieves the minimal half-tilt angle. This is exactly the configuration shown in Fig. 4, leading to a (uniform) maximal leg-singularity-free half-tilt angle, denoted by ψ_L,

$$\psi_L = \pi/2 - \gamma - (\pi/2 - \beta - \mu) = \beta + \mu - \gamma \qquad (16)$$

Taking into consideration different modes of leg singularity of the $\mathcal{UU}$ leg and ranges of constants, we have

$$\psi_L = \min(|\beta + \mu - \gamma|, |\beta - \mu - \gamma|, \\ |\beta + \mu + \gamma - \pi|, |\beta - \mu + \gamma - \pi|) \qquad (17)$$

Static Singularity

A *static singularity* (leading to a loss of control of the PM, [27]) corresponds to the linear dependency of all constraint wrenches $\zeta_{i1}, i = 1, \ldots, N, \zeta_2$ and actuation wrenches ζ_{a1}, ζ_{a1}. If three $\mathcal{UU}$ legs are present, the mechanism is at a static singularity when

$$\begin{bmatrix} \zeta_{11} & \zeta_{21} & \zeta_{31} & \zeta_2 & \zeta_{a1} & \zeta_{a2} \end{bmatrix} = 0 \qquad (18)$$

where $[\,\cdot\,]$ denotes the determinant of a square matrix formed by the vectors within. Since all the constraint and actuation wrenches have zero pitch, we can readily apply the

Grassmann-Cayley Algebra (GCA) techniques [22, 23] to further decompose (18): each constraint or actuation wrench is a 2-extensor joined by two points on the corresponding screw axis

$$\begin{aligned}
\boldsymbol{\zeta}_{11} &= \mathbf{s}_{11}\mathbf{s}_{12} & \boldsymbol{\zeta}_2 &= \mathbf{s}^+\mathbf{s}^- \\
\boldsymbol{\zeta}_{21} &= \mathbf{s}_{21}\mathbf{s}_{22} & \boldsymbol{\zeta}_{a1} &= \mathbf{s}_{12}\mathbf{s}^- \\
\boldsymbol{\zeta}_{31} &= \mathbf{s}_{31}\mathbf{s}_{32} & \boldsymbol{\zeta}_{a2} &= \mathbf{s}_{22}\mathbf{s}^-
\end{aligned} \tag{19}$$

Then Eqn. (18) is equivalent to the following *superbracket* being zero:

$$[[\,\mathbf{s}_{11}\mathbf{s}_{12}\,,\,\mathbf{s}_{21}\mathbf{s}_{22}\,,\,\mathbf{s}_{31}\mathbf{s}_{32}\,,\,\mathbf{s}^+\mathbf{s}^-\,,\,\mathbf{s}_{12}\mathbf{s}^-\,,\,\mathbf{s}_{22}\mathbf{s}^-\,]] = 0 \tag{20}$$

which may be factorized in 24 monomials. Note in particular the repeated occurrence of $\mathbf{s}^-$ will send most monomials to zero, resulting in the following simple identity involving determinants of 4×4 (using homogeneous point coordinates) instead of 6×6 matrices:

$$\left[\mathbf{s}_{11}\ \mathbf{s}_{12}\ \mathbf{s}^-\ \overset{\bullet}{\mathbf{s}}_{21}\right] \cdot \left[\overset{\bullet}{\mathbf{s}}_{22}\ \mathbf{s}_{31}\ \mathbf{s}_{32}\ \mathbf{s}^-\right] \cdot \left[\mathbf{s}^+\ \mathbf{s}_{12}\ \mathbf{s}_{22}\ \mathbf{s}^-\right] = 0 \tag{21}$$

where $\left[\mathbf{s}_{11}\ \mathbf{s}_{12}\ \mathbf{s}^-\ \overset{\bullet}{\mathbf{s}}_{21}\right] \cdot \left[\overset{\bullet}{\mathbf{s}}_{22}\ \mathbf{s}_{31}\ \mathbf{s}_{32}\ \mathbf{s}^-\right]$ stands for [22]:

$$\begin{aligned}
&\left[\mathbf{s}_{11}\ \mathbf{s}_{12}\ \mathbf{s}^-\ \mathbf{s}_{21}\right] \cdot \left[\mathbf{s}_{22}\ \mathbf{s}_{31}\ \mathbf{s}_{32}\ \mathbf{s}^-\right] - \\
&\left[\mathbf{s}_{11}\ \mathbf{s}_{12}\ \mathbf{s}^-\ \mathbf{s}_{22}\right] \cdot \left[\mathbf{s}_{21}\ \mathbf{s}_{31}\ \mathbf{s}_{32}\ \mathbf{s}^-\right]
\end{aligned} \tag{22}$$

Therefore the static singularity factorizes into two of its factors being zero:

1. $$\left[\mathbf{s}^+\ \mathbf{s}_{12}\ \mathbf{s}_{22}\ \mathbf{s}^-\right] = 0 \tag{23}$$

which corresponds to the case where $\boldsymbol{\zeta}_{a1}, \boldsymbol{\zeta}_{a2}$ and $\boldsymbol{\zeta}_2$ become coplanar and hence the actuation wrench space $\mathrm{span}(\boldsymbol{\zeta}_{a1}, \boldsymbol{\zeta}_{a2})$ becomes linearly dependent with the constraint wrench space $\mathrm{span}(\boldsymbol{\zeta}_{11}, \boldsymbol{\zeta}_{21}, \boldsymbol{\zeta}_{31}, \boldsymbol{\zeta}_2)$. It is straightforward to deduce, from mirror-symmetry, that Eqn. (23) is equivalent to (ignoring w.l.o.g. the case $\mathbf{s}_{12} = \mathbf{s}_{22}$)

$$\mathbf{s}_{12} + \mathbf{s}_{22} = \mathbf{s}^+ + \mathbf{s}^- \tag{24}$$

This is usually referred to as actuation or *active constraint* singularity [27]. Figure 5 illustrates a 3-$\mathcal{UU}$ PM at a configuration of active constraint singularity. At such a configuration, the constraint wrench $\boldsymbol{\zeta}_2$ (blue arrow) may be represented as linear combination of the two actuation wrenches $\boldsymbol{\zeta}_{a1}, \boldsymbol{\zeta}_{a2}$ (red arrows).

2. $$\left[\mathbf{s}_{11}\ \mathbf{s}_{12}\ \mathbf{s}^-\ \overset{\bullet}{\mathbf{s}}_{21}\right] \cdot \left[\overset{\bullet}{\mathbf{s}}_{22}\ \mathbf{s}_{31}\ \mathbf{s}_{32}\ \mathbf{s}^-\right] = 0 \tag{25}$$

which can be shown to be equivalent to:

$$(\mathbf{s}_{31}\mathbf{s}_{32}\mathbf{s}^- \wedge \mathbf{s}_{11}\mathbf{s}_{12}\mathbf{s}^-) \wedge \mathbf{s}_{21}\mathbf{s}_{22} = 0 \tag{26}$$
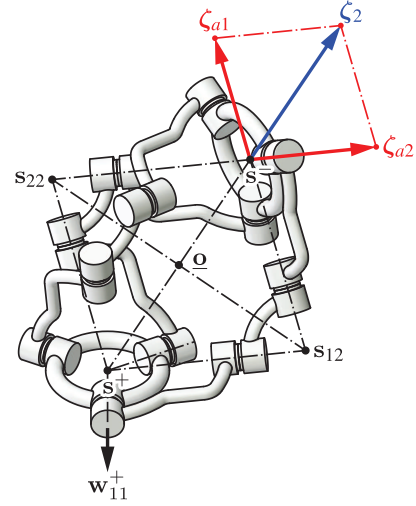

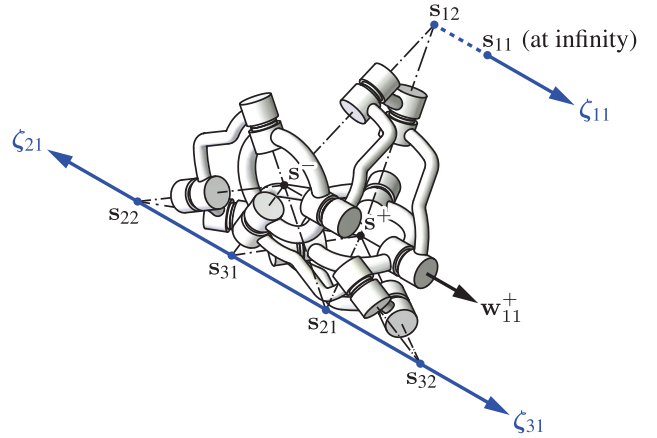Fig. 5. A configuration of active constraint singularity for a 3-$\mathcal{UU}$ PM ($\alpha = 90°$, $\beta = 0°$, $\gamma = 40°$).

Fig. 6. A configuration of passive constraint singularity for a 3-$\mathcal{UU}$ PM ($\alpha = 90°$, $\beta = 0°$, $\gamma = 20°$).

where $\mathbf{s}_{31}\mathbf{s}_{32}\mathbf{s}^-$ and $\mathbf{s}_{11}\mathbf{s}_{12}\mathbf{s}^-$ are 3-extensors, geometrically corresponding to planes passing through the three point members, and $\wedge$ is the *meet operator* [22]. Therefore, Eqn. (26) implies that the line of intersection of $\mathbf{s}_{31}\mathbf{s}_{32}\mathbf{s}^-$ and $\mathbf{s}_{11}\mathbf{s}_{12}\mathbf{s}^-$ intersects with the line $\mathbf{s}_{21}\mathbf{s}_{22}$. Equation (26) may be further simplified into

$$((\mathbf{s}_{31}\mathbf{s}_{32} \wedge \mathbf{s}_{11}\mathbf{s}_{12})\mathbf{s}^-) \wedge \mathbf{s}_{21}\mathbf{s}_{22} = 0 \tag{27}$$

Notice that $\mathbf{s}_{21}\mathbf{s}_{22}$ is completely contained in the symmetry plane as are $\mathbf{s}_{31}\mathbf{s}_{32}$ and $\mathbf{s}_{11}\mathbf{s}_{12}$, we have:

$$(\mathbf{s}_{31}\mathbf{s}_{32} \wedge \mathbf{s}_{11}\mathbf{s}_{12}) \wedge \mathbf{s}_{21}\mathbf{s}_{22} = 0 \tag{28}$$

Equation (28) corresponds to the geometric condition of $\boldsymbol{\zeta}_{11}, \boldsymbol{\zeta}_{21}$ and $\boldsymbol{\zeta}_{31}$ becoming concurrent, and therefore characterizes the (passive) constraint singularity [27]. Figure 6 illustrates a 3-$\mathcal{UU}$ PM at a configuration of passive constraint singularity. In this particular case, $\mathbf{s}_{21}$,

$\mathbf{s}_{22}$, $\mathbf{s}_{31}$ and $\mathbf{s}_{32}$ become collinear and therefore ζ_{21} and ζ_{31} become linearly dependent.

Comparison with the Collapsed N-$\mathcal{UU}$ PM

In [15], we introduced a collapsed N-$\mathcal{UU}$ PM, where each leg is a spherical chain $(\mathbf{w}_{i1}^+, \mathbf{w}_{i2}^+, \mathbf{w}_{12}^-, \mathbf{w}_{11}^-)$, and moreover, $\mathbf{w}_{i2}^+ = \mathbf{w}_{12}^-$. When N = 3, we have shown that its constraint singularity is given by the following identity:

$$\left[\mathbf{w}_{11}^- \times \mathbf{w}_{12}^-, \mathbf{w}_{21}^- \times \mathbf{w}_{22}^-, \mathbf{w}_{31}^- \times \mathbf{w}_{32}^- \right] = 0 \qquad (29)$$

We now show that Eqn. (29) and Eqn. (28) are in fact equivalent when the non-collapsed 3-$\mathcal{UU}$ PM is away from active constraint singularity: this is equivalent to ζ_{a1}, ζ_{a2} and ζ_2 spanning a bundle of forces passing through $\mathbf{s}^-$. As such, the remaining wrenches ζ_{11}, ζ_{21} and ζ_{31} should span a 3-d torque space about $\mathbf{s}^-$ were it be free of constraint singularity. The constraint singularity is then characterized by Eqn. (29) since the torques generated by ζ_{i1}'s, $i = 1, 2, 3$ about $\mathbf{s}^-$ are exactly along the vector $\mathbf{w}_{i1}^- \times \mathbf{w}_{i2}^-$'s.

We remark that in the case of the collapsed N-$\mathcal{UU}$ PM, the singularity will, due to existence of interconnecting links, always factorize into that of the proximal (active constraint) and distal half (passive constraint) of the PM [15]. It is interesting to note that the non-collapsing N-$\mathcal{UU}$ PM enjoys this factorization none the less (although their active constraint singularity differ).

Input-Output Jacobian map of the N-$\mathcal{UU}$ PM

In reference to the remark above, we may simply focus on the pure rotational velocity of the N-$\mathcal{UU}$ PM. Denote the end-effector angular velocity by $\mathbf{w}_{EE}$. We have, due to mirror-symmetry,

$$\begin{aligned}\mathbf{w}_{EE} &= \dot{\theta}_{11}(\mathbf{w}_{11}^+ + \mathbf{w}_{11}^-) + \dot{\theta}_{12}(\mathbf{w}_{12}^+ + \mathbf{w}_{12}^-) \\ &= \dot{\theta}_{21}(\mathbf{w}_{21}^+ + \mathbf{w}_{21}^-) + \dot{\theta}_{22}(\mathbf{w}_{22}^+ + \mathbf{w}_{22}^-)\end{aligned} \qquad (30)$$

where $\dot{\theta}_{12}$ and $\dot{\theta}_{22}$ are unknown passive joint angle speeds. It is straightforward to solve $\dot{\theta}_{12}$ using Eqn. (30), leading to

$$\dot{\theta}_{12} = \dot{\theta}_{21} \underbrace{\frac{\left[\mathbf{w}_{11}^+ + \mathbf{w}_{11}^-, \mathbf{w}_{21}^+ + \mathbf{w}_{21}^-, \mathbf{w}_{22}^+ + \mathbf{w}_{22}^- \right]}{\left[\mathbf{w}_{11}^+ + \mathbf{w}_{11}^-, \mathbf{w}_{12}^+ + \mathbf{w}_{12}^-, \mathbf{w}_{22}^+ + \mathbf{w}_{22}^- \right]}}_{f} \qquad (31)$$

Back substitute in the first equation of Eqn. (30) and we have:

$$\mathbf{w}_{EE} = \underbrace{\left(\mathbf{w}_{11}^+ + \mathbf{w}_{11}^- \quad f(\mathbf{w}_{12}^+ + \mathbf{w}_{12}^-) \right)}_{J_{EE}} \begin{pmatrix} \dot{\theta}_{11} \\ \dot{\theta}_{21} \end{pmatrix} \qquad (32)$$

4 Singularity Loci of 3- and 4-$\mathcal{UU}$ PMs

In this section, we give a complete derivation of the singularity loci of 3- and 4-$\mathcal{UU}$ PMs. To simplify matters, we set $\alpha = 90°$, $\beta = 0°$, which is the configuration adopted by most practical N-$\mathcal{UU}$ PM designs. This particular choice of α and β is confirmed to be (close to being) optimal in terms of maximizing singularity-free workspace of N-$\mathcal{UU}$ PMs [28].

4.1 Leg Singularity Loci

We have already derived the maximal leg-singularity-free half-tilt angle ψ_L in Sec. 3.3, which corresponds to the leg singularity configuration illustrated in Fig. 4. The complete leg singularity locus for leg 1 may simply be derived from the set of all possible direction of $\mathbf{s}^- - \mathbf{s}^+$ while maintaining the rank degeneracy of joint screws. For leg 1, this is given by (from Fig. 4):

$$\begin{aligned} e^{\psi\hat{\mathbf{w}}}(2d\mathbf{z}) &= e^{\theta_{11}\hat{\mathbf{w}}_{11}^+}(\mathbf{s}^- - \mathbf{s}^+) \\ \Leftrightarrow \quad \left(\mathbf{w}_{11}^+\right)^T e^{\psi\hat{\mathbf{w}}}(2d\mathbf{z}) &= \left(\mathbf{w}_{11}^+\right)^T e^{\theta_{11}\hat{\mathbf{w}}_{11}^+}(\mathbf{s}^- - \mathbf{s}^+) \\ &= \left(\mathbf{w}_{11}^+\right)^T (\mathbf{s}^- - \mathbf{s}^+) \end{aligned} \qquad (33)$$

which leads to the following locus, denoted $\Phi_{L,1} = 0$:

$$\begin{aligned}\Phi_{L,1} &= c_\beta s_\phi s_\psi + s_\beta c_\psi + c_\beta s_{\psi_L} - s_\beta c_{\psi_L} \\ &= s_\phi s_\psi + s_{\psi_L}\end{aligned} \qquad (34)$$

where $\psi_L = |\pi/2 - \gamma|$ from Eqn. (17) and $\beta = 0°$ ($\mu = 90°$ as a result). By axial symmetry, the complete leg singularity loci, denoted $\Phi_L = 0$, is given by:

$$\Phi_L = \prod_{i=1}^N \Phi_{L,1}(\phi - (i-1)\phi_0, \psi) = 0, \qquad \phi_0 = 2\pi/N \quad (35)$$

A numerical contouring procedure similar to those in [20,29] may then be applied to Eqn. (35) to plot the leg singularity loci. The leg singularity loci are illustrated in both Fig. 7 and Fig. 8 by gray dash-dot curves.

4.2 Actuation Singularity Loci

We first plug the direct displacement kinematics in Eqn. (23) to attain the following variety describing the actuation singularities:

$$\Phi_A = -s_{\phi_0}^2 c_\psi^2 + s_\gamma^2 c_\phi^2 s_{2\psi}^2 + s_\gamma^2 (s_{\phi_0} - 2c_\phi s_{(\phi-\phi_0)} s_\psi^2)^2 = 0 \quad (24')$$

Numerical contouring procedure may then be applied to Eqn. (24') to plot the loci, an example of which is illustrated by the blue curves in Fig. 7. For the purpose of singularity-free design, we also need to identify the (uniform) maximal actuation-singularity-free tilt angle, which we denote by $2\psi_A$. This can be extracted by the same numerical contouring procedure, and is given by the radius of the maximum inscribed circle (red dashed) of the singularity loci.

It may be shown, by computing Eqn. (24) using inverse displacement kinematics, that the actuation singularity loci
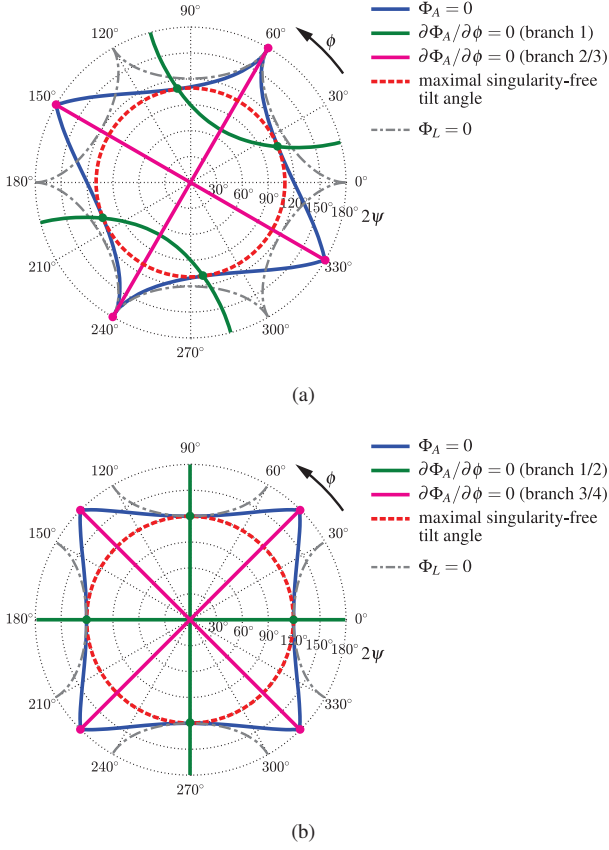
Fig. 7. Active constraint singularity loci of a N-$\mathcal{UU}$ PM and its differential loci ($\gamma = 30°$; coordinates are scaled up to match the true tilt angle 2ψ). (a) N = 3 ($\phi_0 = 120°$); (b) N = 4 ($\phi_0 = 90°$).

shown in Fig. 7 comprises two of four branches that correspond to the two actuating legs each taking one of the two inverse solutions. The two missing branches correspond to the case $s_{12} = s_{22}$ that can only occur at a leg singularity.

Alternatively, we introduce a novel approach to directly compute ψ_A without numerically generating the loci. Note that ψ_A is the extremum of all points on $\Phi_A = 0$ and therefore is necessarily characterized by $\partial\psi/\partial\phi = 0$ since the singularity loci are closed curves (if we identify antipodal points on the boundary of the polar coordinate disk $2\psi = 180°$), which along with

$$\frac{d}{d\phi}\Phi_A(\phi, \psi(\phi)) = \frac{\partial\Phi_A(\phi, \psi)}{\partial\phi} + \frac{\partial\Phi_A(\phi, \psi)}{\partial\psi} \cdot \frac{\partial\psi}{\partial\phi} = 0 \quad (36)$$

implies the following necessary condition:

$$\frac{\partial\Phi_A(\phi, \psi)}{\partial\phi} = 0 \tag{37}$$
$$\Leftrightarrow \quad (2c_{2\psi}s_\phi s_{(\phi-\phi_0)} + c_{(2\phi-\phi_0)} + c_{\phi_0})s_{(2\phi-\phi_0)} = 0$$

As shown in Fig. 7, the differential loci comprise of three branches, the first (green) resulting from $2c_{2\psi}s_\phi s_{(\phi-\phi_0)} +$

$c_{(2\phi-\phi_0)} + c_{\phi_0} = 0$, and the second and third (magenta) resulting from $s_{(2\phi-\phi_0)} = 0$, or $\phi = \phi_0/2 + k\pi/2, k = 0, 1$.

Since the point (ϕ^*, ψ^*) on the loci $\Phi_A = 0$ where $\psi^* = \psi_A$ also lies on the differential loci $\partial\Phi_A/\partial\phi = 0$, ϕ^* is neccesarily a solution of the system of equations $\Phi_A = \partial\Phi_A/\partial\phi = 0$, or Eqn. (37) and Eqn. (24′). This gives rise to at most 8 solutions of ϕ^* such that $\Phi_A(\phi^*, \psi_A) = 0$. For example, in the case of $\gamma = 30°$, as shown in Fig. 7, the active constraint singularity loci (blue) intersect the first set of differential loci (green) at four points, all having the same (uniform) maximal tilt angle $2\psi_A$; it intersects the second set (magenta) at another four points which belong to the minimal enclosing circle (where the wrist achieves maximal singularity-free tilt angle in one particular tilt direction).

4.3 Passive Constraint Singularity Loci

In the case of N = 3, the passive constraint singularity loci, denoted $\Phi_P = 0$, may be derived from Eqn. (29) using inverse displacement kinematics. Its expression is too complex for symbolic reduction and is omitted. In comparison to the active constraint singularity where only two actuating legs are involved, the passive constraint singularity involves all three legs and consequently comprises eight branches, a situation similar to that reported in [29]. An example of passive constraint singularity loci is shown in Fig. 8. In particular, Fig. 8(a) illustrates the branch that corresponds to the mechanism configuration considered in this paper (i.e., as depicted in Fig. 1(a)). It results from assigning positive branch index [29] to all three legs. As in the case of actuation singularity, the (uniform) maximal passive-constraint-singularity-free tilt angle, which we denote by $2\psi_P$, is given by the radius of the maximum inscribed circle (red dashed) of the singularity loci. For completeness, we also illustrate the other seven branches in Fig. 8(b) – (e).

For the case N = 4, passive constraint singularity corresponds to the row rank degeneracy of the following 3×4 matrix:

$$\left(\begin{array}{cccc} \mathbf{w}_{11}^- \times \mathbf{w}_{12}^- & \mathbf{w}_{21}^- \times \mathbf{w}_{22}^- & \mathbf{w}_{31}^- \times \mathbf{w}_{32}^- & \mathbf{w}_{41}^- \times \mathbf{w}_{42}^- \end{array} \right) \tag{38}$$

or geometrically, the concurrence of $\mathbf{s}_{i1}\mathbf{s}_{i2}$, $i = 1, 2, 3, 4$. One may deduce, from the fact $\mathbf{w}_{11}^- = -\mathbf{w}_{31}^-$ and $\mathbf{w}_{21}^- = -\mathbf{w}_{41}^-$, that $\mathbf{s}_{11} = \mathbf{s}_{31}$ and $\mathbf{s}_{21} = \mathbf{s}_{41}$. Therefore, $\mathbf{s}_{i1}\mathbf{s}_{i2}$, $i = 1, 2, 3, 4$ become concurrent only when $\mathbf{s}_{11} = \mathbf{s}_{21}$, which can be ruled out for all cases where $d \neq 0$.

Finally, we would like to comment that, as is illustrated by the case with N = 3 and 4, our synthesis and singularity analysis of N-$\mathcal{UU}$ PMs may be easily generalized to the case where N > 4. The detailed results add little to our study and are therefore omitted.

5 Singularity-Free Design of N-$\mathcal{UU}$ PMs

In this section, we shall utilize our earlier analysis on singularities of a N-$\mathcal{UU}$ PM in its optimal design for maximal singularity-free workspace (prescribed by the maximal uniform singularity-free tilt angle which we denote by ψ_{max}).
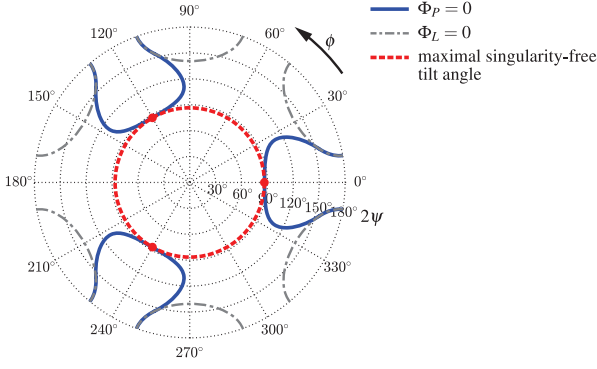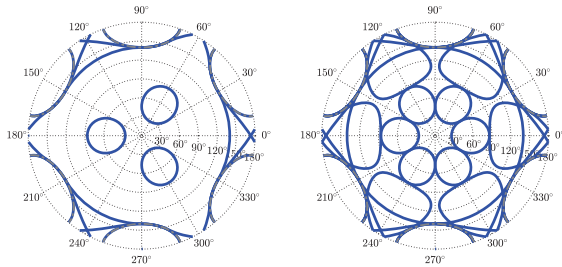
(a) +++
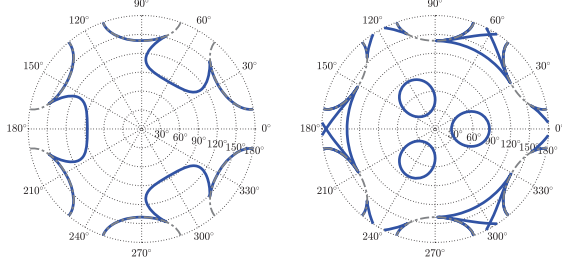
(b) − − −

(c) − + + / + − + / + + −

(d) + − − / − + − / − − +

(e)

Fig. 8. Passive constraint singularity locus of a 3-$\mathcal{UU}$ PM ($\phi_0 = 120°$, $\gamma = 20°$; coordinates are scaled up to match the true tilt angle 2ψ). (a) branch 1; (b) branch 2; (c) branch 3-5; (d) branch 6-8; (e) all branches.

5.1 Choice of Singularity Margin

An appropriate singularity margin should be defined in order to avoid degenerated accuracy and / or stiffness of the N-$\mathcal{UU}$ PM near a singular configuration. Without further information leading to more meaningful singularity measures, we may simply set a margin ψ_{margin} on the half-tilt angle, so that ψ_{max} is given by the minimum of ψ_L, ψ_A and ψ_P for a particular design constant γ subtracted by ψ_{margin}:

$$\psi_{\mathrm{max}}(\gamma) = \min(\psi_L(\gamma), \psi_A(\gamma), \psi_P(\gamma)) - \psi_{\mathrm{margin}} \quad (39)$$

We may find the optimal constant value $\gamma = \gamma_{\mathrm{max}}$ which leads to the maximal tilt angle via a performance atlas of $\psi_{\mathrm{max}}(\gamma)$ versus γ. For N = 3, it can be shown that $\gamma_{\mathrm{max}} = 25.7789°$ (see Fig. 9), which is consistent with the design constant of the Unitru joint [8] ($\gamma = 22.5°$) and Omni-Wrist [9] ($\gamma = 24°$).
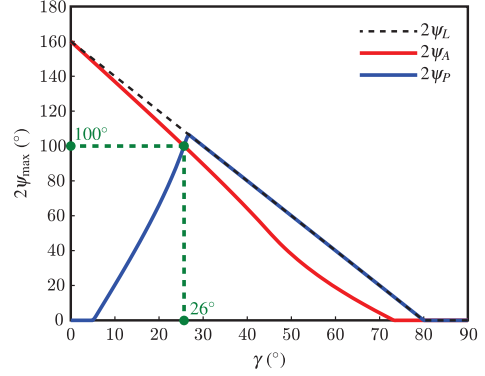

Fig. 9. Distribution of $2\psi_{\mathrm{max}}$ versus γ for a 3-$\mathcal{UU}$ PM using a tilt angle margin of $2\psi_{\mathrm{margin}} = 20°$.

The above approach is based on the numerical contouring procedure, and therefore does not generalize to the case N = 4 where the passive constraint singularity loci vanish. Alternatively, we may set a margin i_{margin} on certain index i that measures closeness to singularity (see for example [30] and the references therein). For example, for N = 3, we may choose i to be the minimum singular value, denoted σ_1, of the matrix with columns corresponding to normalized actuation and constraint torques:

$$\begin{aligned} i_A &= \sigma_1 \left(\mathbf{w}_{12}^- \ \mathbf{w}_{22}^- \ (\mathbf{s}^- - \mathbf{s}^+)/(2d) \right) \\ i_P &= \sigma_1 \left(\mathbf{w}_{11}^- \times \mathbf{w}_{12}^- \ \mathbf{w}_{21}^- \times \mathbf{w}_{22}^- \ \mathbf{w}_{31}^- \times \mathbf{w}_{32}^- \right) \end{aligned} \quad (40)$$

i_A and i_P denote the active and passive constraint singularity index respectively. These are exactly the closeness measure proposed in [31] specializing to the pure rotational case. For N = 4, i_P is simply changed to:

$$i_P = \sigma_1 \left(\mathbf{w}_{11}^- \times \mathbf{w}_{12}^- \ \mathbf{w}_{21}^- \times \mathbf{w}_{22}^- \ \mathbf{w}_{31}^- \times \mathbf{w}_{32}^- \ \mathbf{w}_{41}^- \times \mathbf{w}_{42}^- \right) \quad (41)$$

## 5.2 Identification of Maximal Singularity-free Half-tilt Angle ψ_{max}

To identify the maximal singularity-free half-tilt angle ψ_{max}, we simply apply the same numerical contouring procedure to $i_A = i_{\mathrm{margin}}$ and $i_P = i_{\mathrm{margin}}$ for a specified singularity margin i_{margin}. ψ_{max} is simply identified as the radius of the maximum inscribed circle of the resultant loci. Some relevant details of the procedure are summarized as follows.

First, in order to accelerate the actuation singularity contouring procedure, we shrink the domain of computation to $\phi \in [0, \pi]$, $\psi \in [0, |\pi/2 - \gamma|]$ by noting the two-fold axial symmetry of the loci (cf. Fig. 7) and the fact that ψ_{max} is bounded above by ψ_L. The axial symmetry is a result of the structural symmetry of the mechanism (considering only the two actuating legs). Similarly, we set $\phi \in [0, 2\pi/N]$, $\psi \in [0, |\pi/2 - \gamma|]$ for passive constraint singularity by noting its N-fold axial symmetry due to structural symmetry (cf. Fig. 8).

Next, since the above procedure does not guarantee that the interior of the loci corresponds to an index value greater

(a)

(a)

(b)
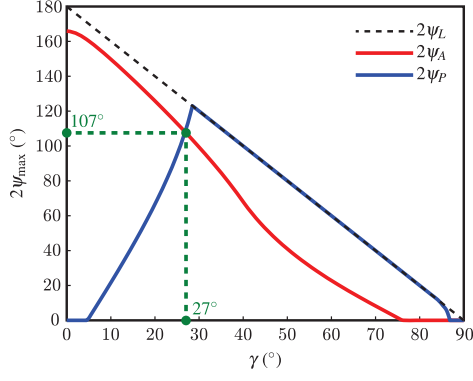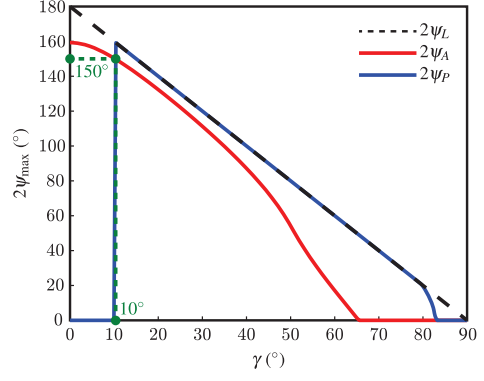
(b)

Fig. 10.   Distribution of $2\psi_{max}$ versus γ for a 3-$\mathcal{UU}$ PM using a singularity margin of (a) $i_{margin} = 0.1$ (b) $i_{margin} = 0.2$.

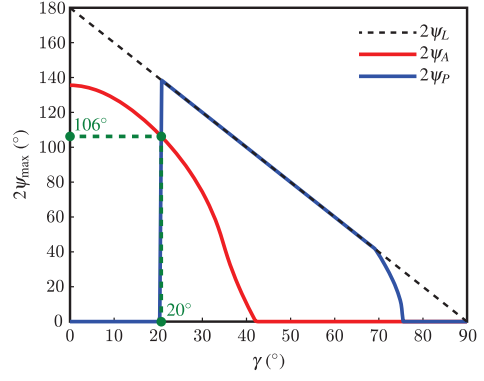Fig. 11.   Distribution of $2\psi_{max}$ versus γ for a 4-$\mathcal{UU}$ PM using a singularity margin of (a) $_{margin} = 0.25$ (b) $i_{margin} = 0.5$.

than i_{margin}, we verify the value of i_A (or i_P) at $\phi = \psi = 0$: if $i_A > i_{margin}$ (or $i_P > i_{margin}$), ψ_{max} is given by the radius of the maximum inscribed circle of the resultant loci; if $i_A < i_{margin}$ (or $i_P < i_{margin}$), ψ_{max} is equal to 0.

The distribution of $2\psi_{max}$ versus γ for a 3-$\mathcal{UU}$ PM using a singularity margin of $i_{margin} = 0.1$ and 0.2 are illustrated in Fig. 10(a) and (b) respectively. The optimal value for γ in these cases are $\approx 27°$ and $\approx 28°$ respectively, which corroborates the result from setting a simple tilt angle margin.

The distribution of $2\psi_{max}$ versus γ for a 4-$\mathcal{UU}$ PM using a singularity margin of $i_{margin} = 0.25$ and 0.5 are illustrated in Fig. 11(a) and (b) respectively. The optimal value for γ in these cases are $\approx 10°$ and $\approx 20°$ respectively. In comparison to the 3-$\mathcal{UU}$ PM, the 4-$\mathcal{UU}$ PM is allowed to have a smaller value in γ due to existence of extra constraint torques. Its optimal workspace also appears to be larger than that of the 3-$\mathcal{UU}$ PM even when a much bigger singularity margin is set. This suggests that 4-$\mathcal{UU}$ PMs should be preferred over 3-$\mathcal{UU}$ PMs for better accuracy and stiffness performance.

6   Conclusion

In this paper, we have conducted a comprehensive analysis of the N-$\mathcal{UU}$ PM with the aim of optimal design for achieving a maximal uniform tilt angle. We have shown that by utilizing the symmetric submanifold properties of its un-

derlying motion manifold, we gain a very clear geometric understanding of both the synthesis condition and the displacement and twist / wrench kinematics of the N-$\mathcal{UU}$ PM. It should be emphasized that this geometric approach is supported by symmetric space theory and therefore generalizable to other PMs involving symmetric submanifolds. We have illustrated this by drawing connection to a collapsed N-$\mathcal{UU}$ PM, which is topologically distinct from the non-collapsing one studied here (the former attains interconnecting links). We remark that the synthesis and analysis approach presented in this paper may be easily generalized to other types of mechanisms whose output motion manifold is a symmetric submanifold, thanks to the mirror-symmetry and half-angle property that universally apply to all symmetric submanifolds of SE(3). However, the spherical reduction of the N-$\mathcal{UU}$ PMs is unlikely to have such a generalization.

References

[1] Murray, R. M., Li, Z., Sastry, S. S., and Sastry, S. S., 1994. *A mathematical introduction to robotic manipulation*. CRC press.

[2] Wu, Y., Löwe, H., Carricato, M., and Li, Z., 2016. "Inversion symmetry of the Euclidean group: Theory and application to robot kinematics". *IEEE Transactions on Robotics*, **32**(2), pp. 312–326.

[3] Hunt, K., 1973. "Constant-velocity shaft couplings: a general theory". *Journal of Engineering for Industry*, **95**(2), pp. 455–464.

[4] Carricato, M., 2009. "Decoupled and homokinetic transmission of rotational motion via constant-velocity joints in closed-chain orientational manipulators". *Journal of Mechanisms and Robotics*, **1**(4), p. 041008.

[5] Wu, Y., Li, Z., and Shi, J., 2010. "Geometric properties of zero-torsion parallel kinematics machines". In Intelligent Robots and Systems (IROS), 2010 IEEE/RSJ International Conference on, IEEE, pp. 2307–2312.

[6] Bonev, I. A., and Ryu, J., 2001. "A new approach to orientation workspace analysis of 6-dof parallel manipulators". *Mechanism and machine theory*, **36**(1), pp. 15–28.

[7] Bonev, I., Zlatanov, D., and Gosselin, C., 2002. "Advantages of the modified Euler angles in the design and control of PKMs". In 2002 Parallel Kinematic Machines International Conference, Citeseer, pp. 171–188.

[8] Culver, I. H., 1969. Constant velocity universal joint, Nov. 11. US Patent 3,477,249.

[9] Rosheim, M. E., and Sauter, G. F., 2002. "New high-angulation omni-directional sensor mount". In International Symposium on Optical Science and Technology, International Society for Optics and Photonics, pp. 163–174.

[10] Sone, K., Isobe, H., and Yamada, K., 2004. "High angle active link". *Special Issue Special Supplement to Industrial Machines*.

[11] Kong, X., Yu, J., and Li, D., 2016. "Reconfiguration analysis of a two degrees-of-freedom 3-4R parallel manipulator with planar base and platform". *Journal of Mechanisms and Robotics*, **8**(1), p. 011019.

[12] Löwe, H., Wu, Y., and Carricato, M., 2016. "Symmetric subspaces of SE(3)". *Advances in Geometry*, **16**(3), pp. 381–388.

[13] Wu, Y., and Carricato, M., 2017. "Identification and geometric characterization of Lie triple screw systems and their exponential images". *Mechanism and Machine Theory*, **107**, pp. 305–323.

[14] Wu, Y., Müller, A., and Carricato, M., 2016. "The 2D orientation interpolation problem: a symmetric space approach". In Advances in Robot Kinematics, Springer.

[15] Wu, Y., and Carricato, M., 2015. "Design of a novel 3-DoF serial-parallel robotic wrist: A symmetric space approach". In Proceedings of the International Symposium on Robotics Research (ISRR 2015), Sestri Levante, Italy, Springer.

[16] Sofka, J., Skormin, V., Nikulin, V., and Nicholson, D., 2006. "Omni-wrist III-a new generation of pointing devices. part I. laser beam steering devices-mathematical modeling". *IEEE Transactions on Aerospace and Electronic Systems*, **42**(2), pp. 718–725.

[17] Yu, J., Dong, X., Pei, X., and Kong, X., 2012. "Mobility and singularity analysis of a class of two degrees of freedom rotational parallel mechanisms using a visual graphic approach". *Journal of Mechanisms and Robotics*, **4**(4), p. 041006.

[18] Wu, K., Yu, J., Zong, G., and Kong, X., 2014. "A family of rotational parallel manipulators with equal-diameter spherical pure rotation". *Journal of Mechanisms and Robotics*, **6**(1), p. 011008.

[19] Kong, X., and Yu, J., 2015. "Type synthesis of two-degrees-of-freedom 3-4R parallel mechanisms with both spherical translation mode and sphere-on-sphere rolling mode". *Journal of Mechanisms and Robotics*, **7**(4), p. 041018.

[20] Bonev, I. A., and Gosselin, C. M., 2005. "Singularity loci of spherical parallel mechanisms". In IEEE International Conference on Robotics and Automation, Vol. 3, IEEE; 1999, p. 2957.

[21] Briot, S., and Bonev, I. A., 2008. "Singularity analysis of zero-torsion parallel mechanisms". In Intelligent Robots and Systems, 2008. IROS 2008. IEEE/RSJ International Conference on, IEEE, pp. 1952–1957.

[22] Ben-Horin, P., and Shoham, M., 2009. "Application of Grassmann–Cayley algebra to geometrical interpretation of parallel robot singularities". *The International Journal of Robotics Research*, **28**(1), pp. 127–141.

[23] Kanaan, D., Wenger, P., Caro, S., and Chablat, D., 2009. "Singularity analysis of lower mobility parallel manipulators using Grassmann–Cayley algebra". *IEEE Transactions on Robotics*, **25**(5), pp. 995–1004.

[24] Hunt, K. H., 1978. *Kinematic geometry of mechanisms*. Oxford University Press, USA.

[25] Meng, J., Liu, G., and Li, Z., 2007. "A geometric theory for analysis and synthesis of sub-6 dof parallel manipulators". *IEEE Transactions on Robotics*, **23**(4), pp. 625–649.

[26] Selig, J., 2016. "Some mobile overconstrained parallel mechanisms". In Advances in Robot Kinematics (ARK 2016), June 27–30, Grasse, France.

[27] Conconi, M., and Carricato, M., 2009. "A new assessment of singularities of parallel kinematic chains". *IEEE Transactions on Robotics*, **25**(4), pp. 757–770.

[28] Wu, Y., and Carricato, M., 2017. "Optimal design of N-$\mathcal{UU}$ parallel mechanisms". In 7th IFTOMM International Workshop on Computational Kinematics, May 22–24, Futuroscope-Poitiers, France.

[29] Bonev, I. A., and Gosselin, C. M., 2001. "Singularity loci of planar parallel manipulators with revolute joints". In 2nd Workshop on Computational Kinematics, pp. 20–22.

[30] Merlet, J.-P., 2012. *Parallel robots*. Springer Science & Business Media.

[31] Voglewede, P. A., and Ebert-Uphoff, I., 2005. "Overar-

ching framework for measuring closeness to singular-ities of parallel manipulators". *IEEE Transactions on Robotics,* **21**(6), pp. 1037–1045.

[32] Pottmann, H., Peternell, M., and Ravani, B., 1999. "An introduction to line geometry with applications". *Computer-aided design,* **31**(1), pp. 3–16.

Appendix A: Displacement Kinematics of the N-$\mathcal{U}\mathcal{U}$ PM

Inverse Displacement Kinematics

Given a desired tilt axis $\mathbf{w} = \mathbf{x}c_\phi + \mathbf{y}s_\phi$ and half-tilt angle ψ, we first compute the current location of the distal center $\mathbf{s}^-$

$$\mathbf{s}^- = \mathbf{s}^-(\phi, \psi) = e^{\psi\widehat{\mathbf{w}}}(2d\mathbf{z}) + \mathbf{s}^+ \qquad (42)$$

which may then be used to compute $\mathbf{s}_{i2}$, $i = 1,\ldots,N$. More specifically, $\mathbf{s}_{i2}$ satisfies the following two linear equations, the first resulting from the mirror-symmetry of the $\mathcal{U}\mathcal{U}$ leg (see Fig. 3(a))

$$(\mathbf{s}^- - \mathbf{s}^+)^T (\mathbf{s}_{i2} - \underbrace{(\mathbf{s}^- + \mathbf{s}^+)/2}_{\mathbf{o}}) = 0 \qquad (43)$$

and the second resulting from link geometry (Fig. 1(d))

$$(e^{2\psi\widehat{\mathbf{w}}}\mathbf{w}_{i1}^-)^T (\mathbf{s}_{i2} - \mathbf{s}^-) = c_\mu d/s_\gamma \qquad (44)$$

$\mathbf{s}_{i2}$ lies on the line of intersection of the two planes prescribed by Eqn. (43) and Eqn. (44), with Plücker coordinate [32]

$$\mathbf{l} = \mathbf{u} \times \mathbf{v}, \qquad \bar{\mathbf{l}} = u_0\mathbf{v} - v_0\mathbf{u} \qquad (45)$$

with

$$\begin{aligned} \mathbf{u} &= \mathbf{s}^- - \mathbf{s}^+, \quad \mathbf{v} = e^{2\psi\widehat{\mathbf{w}}}\mathbf{w}_{i1}^- \\ u_0 &= -(\mathbf{s}^- - \mathbf{s}^+)^T(\mathbf{s}^- + \mathbf{s}^+)/2 \\ v_0 &= -(e^{2\psi\widehat{\mathbf{w}}}\mathbf{w}_{i1}^-)^T\mathbf{s}^- - c_\mu d/s_\gamma \end{aligned} \qquad (46)$$

This allows us to express $\mathbf{s}_{i2}$ by

$$\mathbf{s}_{i2} = \mathbf{s}_{i2}(\lambda) = \begin{cases} (\mathbf{l} \times \bar{\mathbf{l}})/\|\mathbf{l}\|^2 + \lambda\mathbf{l} & \mathbf{l} \neq \mathbf{0} \\ \lambda\bar{\mathbf{l}} & \mathbf{l} = \mathbf{0} \end{cases} \quad \lambda \in \mathbb{R} \qquad (47)$$

where $\|\mathbf{l}\| = (\mathbf{l}^T\mathbf{l})^{1/2}$. We may solve the unknown λ from the following quadratic equation which results again from link geometry:

$$(\mathbf{s}_{i2}(\lambda) - \mathbf{s}^+)^T (\mathbf{s}_{i2}(\lambda) - \mathbf{s}^+) = d^2/s_\gamma^2 \qquad (48)$$

Note that this is a quadratic equation in λ, we have up to two solutions for each $\mathbf{s}_{i2}$. The input angles $(\theta_{11}, \theta_{21})$ may finally be derived from link geometry, and is given by

$$\left(\frac{\mathbf{s}_{i2} - \mathbf{s}^-}{\|\mathbf{s}_{i2} - \mathbf{s}^-\|} - \mathbf{w}_{i1}^+ c_\mu \right)^T \left(\mathbf{w}_{i2}^+ - \mathbf{w}_{i1}^+ c_\mu \right) = s_\mu^2 c_{\theta_{i1}}, \ i = 1, 2 \qquad (49)$$

Direct Displacement Kinematics

The direct displacement kinematics may be derived by reversing the inverse displacement kinematics. First, given the input angles $(\theta_{11}, \theta_{21})$, we may compute $\mathbf{s}_{i2}$, $i = 1, 2$ by

$$\mathbf{s}_{i2} = \mathbf{s}_{i2}(\theta_{11}, \theta_{21}) = e^{\theta_{i1}\widehat{\mathbf{w}}_{i1}^+}\mathbf{s}_{i2} \qquad (50)$$

Two linear equations for $\mathbf{s}^-$ may then be extracted from taking the differences of the following three equations resulting from link geometry

$$\begin{aligned} (\mathbf{s}^- - \mathbf{s}^+)^T (\mathbf{s}^- - \mathbf{s}^+)^T &= 4d^2 \\ (\mathbf{s}^- - \mathbf{s}_{11})^T (\mathbf{s}^- - \mathbf{s}_{11}) &= d^2/s_\gamma^2 \\ (\mathbf{s}^- - \mathbf{s}_{21})^T (\mathbf{s}^- - \mathbf{s}_{21}) &= d^2/s_\gamma^2 \end{aligned} \qquad (51)$$

Rewriting $\mathbf{s}^-$ using Plücker coordinate of the intersection line and back-substituting into one of the three equations in Eqn. (51) gives two solutions of $\mathbf{s}^-$. The tilt axis $\mathbf{w}$ and half-tilt angle ψ may then be easily derived using Eqn. (42). □